


Non-invasive *in vivo* imaging of acute thrombosis: development of a novel factor XIIIa radiotracer

Jack P.M. Andrews ^{1*}, Christophe Portal², Tashfeen Walton³, Mark G. Macaskill¹, Patrick W.F. Hadoke¹, Carlos Alcaide Corral¹, Christophe Lucatelli³, Simon Wilson¹, Ian Wilson⁴, Gillian MacNaught³, Marc R. Dweck¹, David E. Newby¹, and Adriana A.S. Tavares¹

¹BHF Centre for Cardiovascular Science, University of Edinburgh, 49 Little France Crescent, Edinburgh, UK; ²Edinburgh Molecular Imaging Ltd., 9 Little France Road, Edinburgh, UK; ³Edinburgh Imaging facility QMRI, University of Edinburgh, 47 Little France Crescent, Edinburgh, UK; and ⁴ImaginAb, Inc. U.S. 43 Hindry Avenue, Suite D, Inglewood, California, USA

Received 8 May 2019; editorial decision 19 July 2019; accepted 7 August 2019; online publish-ahead-of-print 13 August 2019

Aims

Cardiovascular thrombosis is responsible a quarter of deaths annually worldwide. Current imaging methods for cardiovascular thrombosis focus on anatomical identification of thrombus but cannot determine thrombus age or activity. Molecular imaging techniques hold promise for identification and quantification of thrombosis *in vivo*. Our objective was to assess a novel optical and positron-emitting probe targeting Factor XIIIa (ENC2015) as biomarker of active thrombus formation.

Methods and results

Optical and positron-emitting ENC2015 probes were assessed *ex vivo* using blood drawn from human volunteers and passed through perfusion chambers containing denuded porcine aorta as a model of arterial injury. Specificity of ENC2015 was established with co-infusion of a factor XIIIa inhibitor. *In vivo* ¹⁸F-ENC2015 biodistribution, kinetics, radiometabolism, and thrombus binding were characterized in rats. Both Cy5 and fluorine-18 labelled ENC2015 rapidly and specifically bound to thrombi. Thrombus uptake was inhibited by a factor XIIIa inhibitor. ¹⁸F-ENC2015 remained unmetabolized over 8 h when incubated in *ex vivo* human blood. *In vivo*, 42% of parent radiotracer remained in blood 60 min post-administration. Biodistribution studies demonstrated rapid clearance from tissues with elimination via the urinary system. *In vivo*, ¹⁸F-ENC2015 uptake was markedly increased in the thrombosed carotid artery compared to the contralateral patent artery (mean standard uptake value ratio of 2.40 vs. 0.74, $P < 0.0001$).

Conclusion

ENC2015 rapidly and selectively binds to acute thrombus in both an *ex vivo* human translational model and an *in vivo* rodent model of arterial thrombosis. This probe holds promise for the non-invasive identification of thrombus formation in cardiovascular disease.

Keywords

Positron emission tomography • Thrombus • Thrombosis • Atherothrombosis • Radiotracer • PET/CT

Introduction

Acute vascular thrombosis is common to the pathogenesis of myocardial infarction, stroke, and venous thromboembolism which collectively are responsible for a quarter of all deaths annually worldwide.¹ At present, imaging approaches to the detection of

acute thrombosis consist mainly of thrombus visualization with ultrasound, invasive catheterization, computerized tomography (CT), and magnetic resonance angiography. Common to all of these imaging modalities is a lack of sensitivity and specificity for acute thrombus detection.^{2–4} None can accurately ascertain whether a thrombus is physiologically active or dormant which can

* Corresponding author. Tel: +44 (77) 6688 5010; Fax: +131 242 6379. E-mail: Jack.Andrews@ed.ac.uk

© The Author(s) 2019. Published by Oxford University Press on behalf of the European Society of Cardiology.

This is an Open Access article distributed under the terms of the Creative Commons Attribution Non-Commercial License (<http://creativecommons.org/licenses/by-nc/4.0/>), which permits non-commercial re-use, distribution, and reproduction in any medium, provided the original work is properly cited. For commercial re-use, please contact journals.permissions@oup.com

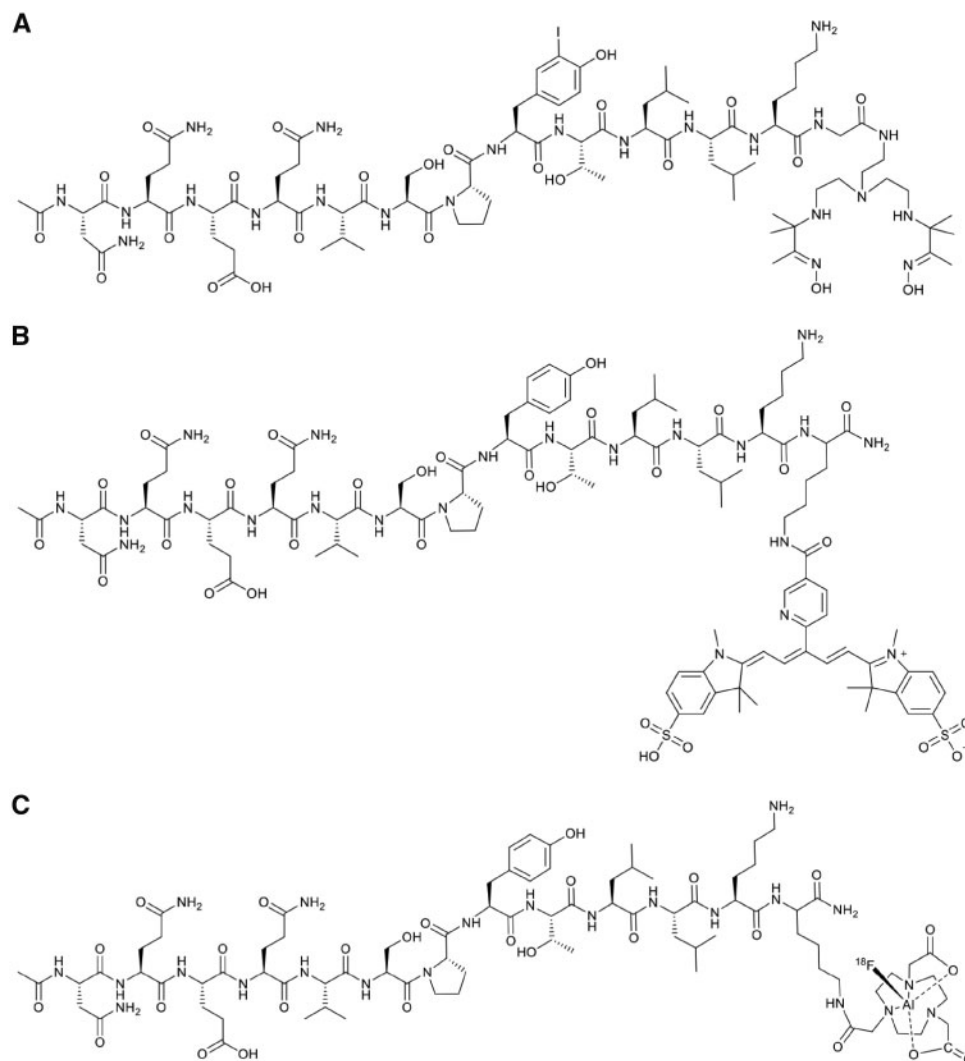


Figure 1 Cy5 and fluorine-18 labelled chemical structure of ENC2015 compound. (A) The chemical structure of NC100668 upon which ENC2015 is based.^{8,9} (B) The ENC2015 peptide with the optical Cy5 label. (C) The ENC2015 peptide after chelation with $Al^{18}F$.

make diagnostic and management decisions regarding anti-thrombotic therapy difficult. These limitations support the development of novel imaging techniques to detect acute vascular thrombosis with greater precision.⁵

Molecular positron emission tomography (PET) imaging offers the potential to address a number of these issues through visualization and quantification of physiological thrombus activity.⁵ Thrombus tracers have so far shown promise in monitoring thrombolysis efficacy in rats⁶ and the detection of acute deep vein thrombosis and pulmonary embolism in humans.⁷ However, none of these PET radiotracers targets the coagulation factor XIIIa (FXIIIa). In the present study, we report on the development of a novel factor XIIIa-directed optical and PET radiotracer, ENC2015 (Figure 1),^{8,9} for the non-invasive imaging of thrombosis *in vivo*. ENC2015 is based on ^{99m}Tc -NC100668, a small single-photon emission computerized tomography (SPECT) FXIIIa-targeted radiotracer. The coagulation factor FXIIIa acts to strengthen fibrin crosslinking in newly formed

thrombus, thus serving as a valuable target to assess thrombus activity and age. Previously, binding of NC100668 to thrombus has been demonstrated in *in vitro* plasma clot assays, a rat model of inferior vena cava thrombosis, and human autopsy specimens of pulmonary thromboemboli.^{10,11} In contrast to NC100668, ENC2015 is labelled with the PET radioisotope fluorine-18 thus allowing for clinical imaging datasets with higher resolution and improved quantification compared with SPECT. Furthermore, ENC2015 was developed as both an optical near-infrared fluorescent probe and an ^{18}F positron-emitting radiotracer to image thrombosis *in vivo*. A dual optical-PET labelled probe would hold great promise for *in vivo* diagnosis and histological tissue validation with a single chemical moiety. Moreover, ENC2015 offers the potential to allow identification of disease before clinical manifestation, track thrombus activity over time, and monitor therapeutic efficacy. Here, we report our pre-clinical assessment of ENC2015 in an *ex vivo* model of human thrombosis and an *in vivo* rodent carotid thrombosis model.

Methods

Synthesis of ENC2015

The peptide scaffold of ENC2015 was prepared by Fmoc solid-phase peptide synthesis using Rink amide Chemmatrix resin and HBTU/DIPEA assisted couplings, monitored by Kaiser ninhydrin test and regular test cleavages followed by HPLC and MALDI-TOF MS analyses. After the assembly of the peptide and capping with Ac_2O , the ϵ -amine Mmt protecting group on the Lysine residue at the C-terminus was deprotected on resin and derivatised with sulfo Cy5 using PyBop as a coupling reagent. Cy5-ENC2015 was obtained after cleaving off the peptide from the solid support and semi-preparative HPLC purification in low yield (4% overall yield) but excellent purity (>98% at 210 nm). The peptide precursor of Al^{18}F -ENC2015 [peptide with *p*-SCN-Bn-1,4,7-triazacyclononane-1,4,7-triacetic acid (NOTA) chelator] was prepared by Fmoc solid-phase peptide synthesis using Rink amide Chemmatrix resin and HBTU/DIPEA assisted couplings, monitored by Kaiser ninhydrin test and regular test cleavages followed by HPLC and MALDI-TOF MS analyses. After the assembly of the peptide and capping with Ac_2O , the ϵ -amine Dde protecting group on the Lysine residue at the C terminus was de-protected on resin and derivatised with NOTA-NHS. The precursor was obtained after cleavage from the solid support and purifying it by semi-preparative HPLC purification in low yield (5% overall yield) but excellent purity (>97% at 210 nm).

Radiolabelling of ENC2015

The radiosynthesis of ^{18}F -ENC2015 was performed at Edinburgh Imaging Facility on a commercial synthesizer, GE TRACERlab[®] MX. A disposable kit was assembled to allow the peptide conjugate to chelate with aluminium fluoride and undergo purification using an automated method. Purified Fluoride-18 (using SepPak QMA Light cartridge eluted with 300 μL saline, ca. 10 GBq) was added to a mixture of NOTA-peptide (12 μL , 2 mM solution in NaOAc buffer pH 4) in the presence of AlCl_3 (6 μL , 2 mM in NaOAc buffer pH 4). Acetonitrile was used as an organic co-solvent (aqueous solution to organic solvent ratio of 1:1.2 v/v) and the mixture was heated to 100°C for 10 min. The reaction mixture was diluted with water (20 mL) and passed through a SepPak Light C18 cartridge (pre-conditioned with ethanol and water). The C18 cartridge was washed with water (2 \times 20 mL) and product was eluted with ethanol (1.5 mL). The final product was formulated in a physiological solution containing 10% ethanol in normal saline. ^{18}F -ENC2015 was obtained with an average non-decay corrected yield of $27 \pm 11\%$ (starting from 10 ± 6 GBq of fluoride-18, $n = 15$) after a total synthesis time of 28 min. Identity of ^{18}F -ENC2015 and its radiochemical purity (>99%) were determined by analytical HPLC (C18, 250 \times 4.6 mm, 1 mL/min, UV absorbance at $\lambda = 267$ nm) at the end of the synthesis. ^{18}F -ENC2015 specific activity was >45 GBq/ μmol .

Ex vivo translational model of human thrombus formation

To confirm target engagement, we examined binding of ENC2015 to newly formed thrombus using an *ex vivo* translational model of acute thrombus formation (Supplementary data online, Figure S1) as described previously.^{12–15} In brief, a pump (Masterflex model 7013, Cole-Palmer Instruments, USA) was used to draw native (un-anticoagulated) blood from the antecubital vein of healthy volunteers through a series of three cylindrical perfusion chambers maintained at 37°C in a water bath. Each chamber contained a carefully prepared strip of porcine aorta (Pel-Freez Biologicals, CA, USA) from which the intima and a thin layer of media had

been removed. Rheological conditions in the first chamber simulated those of patent medium-sized coronary arteries (low-shear rate, 212 s^{-1}), whereas those in the second and third chambers simulated those of mild to moderately stenosed coronary arteries (high shear rate, 1690 s^{-1}). Each study lasted for exactly 5 min during which flow was maintained at a constant rate of 10 mL/min. Following perfusion of blood, the chambers were perfused with 0.9% saline for one minute under the same rheological conditions. Thereafter, the porcine strips with thrombus attached were removed and fixed in 4% paraformaldehyde for 24 h at 4°C prior to being prepared for histological analysis.

Sixteen healthy male volunteers (31 ± 1.26 years) were enrolled into the study which was performed with the approval of the local research ethics committee (AMREC; 17-HV-033), in accordance with the Declaration of Helsinki, and the written informed consent of all the volunteers. Exclusion criteria were history of bleeding diathesis, use of regular medication or any clinically significant illness. We conducted the study in a series of sequences: (i) infusion of Cy5-ENC2015 (250 nM, $n = 6$) or ^{18}F -ENC2015 (4.6 ± 0.5 MBq/mL, $n = 10$); (ii) infusion of Cy5-ENC2015 (250 nM, $n = 6$) or ^{18}F -ENC2015 (5.5 ± 0.9 MBq/mL, $n = 10$) plus factor XIIIa inhibitor (Iodoacetamide, Sigma-Aldrich, UK) at a concentration 10 mg/mL; and (iii) blood control without infusion of optical or radiolabelled tracer ($n = 6$). For the optical probe, further control experimental groups included: (iv) the administration of ENC2015 in the absence of blood, (v) the infusion of free Cy5 fluorophore, and (vi) the infusion of a scrambled peptide sequence (Supplementary data online, Figure S2B) in the presence of thrombus. In one volunteer, we collected blood through the chamber for HPLC radiometabolite analysis to assess tracer stability in *ex vivo* human blood at 0 and 8 h after radiotracer incubation. Furthermore, paraffin-embedded cross-sections of *ex vivo* human thrombi ($n = 3$) were prepared for autoradiographic experiments performed in quadruplicate; (i) ^{18}F -ENC2015; (ii) ^{18}F -ENC2015 co-incubated with homologous unlabelled 'cold' ENC2015 (5 μM); (iii) ^{18}F -ENC2015 co-incubated with heterologous scrambled tracer (5 μM); and (iv) ^{18}F -ENC2015 co-incubated with iodoacetamide (5 μM), a non-selective irreversible inhibitor of all cysteine peptidases, which in this experimental design works as negative control. All tissue sections were de-paraffinized, rehydrated and incubated for 2 h at 37°C, and then slides were washed twice with phosphate buffer solution before being air-dried and exposed to a Fujifilm BAS-IP MS 2040 phosphor screen (Fujifilm, Japan).

Porcine aortic strips from the Badimon chamber experiments were imaged for macroscopic (Biospace Lab PhotonIMAGER Optima system, France) and microscopic thrombus fluorescence (Zeiss Axio Scan.Z1, Germany) on the Cy5 channel (645/670 nm wavelength excitation and emission). Strips exposed to ^{18}F -ENC2015 were imaged with the nanopositron emission tomography-computed tomography (NanoPET/CT, Mediso, Hungary) enabling quantification of tracer uptake. Phosphor screens were imaged on a Fujifilm FLA5100 imaging plate reader (Fujifilm, Japan).

Animal studies

All experiments were conducted in accordance with institutional animal care protocols, authorized by the Home Office under the Animals (Scientific Procedures) Act 1986 and conformed to EU guidelines (Directive 2010/63/EU) of the European Parliament on the protection of animals used for scientific purposes. Adult male rats (16.7 ± 3.8 weeks, 392.8 ± 74.1 g, $n = 8$) were anaesthetized with 2–2.5% isoflurane (50/50 oxygen/nitrous oxide, 1 L/min). Body temperature was maintained by heated scanner bed or heated mat and monitored by a rectal thermometer. Vital signs including heart rate and respiration rate were monitored continuously during the experiments. Biodistribution was assessed in

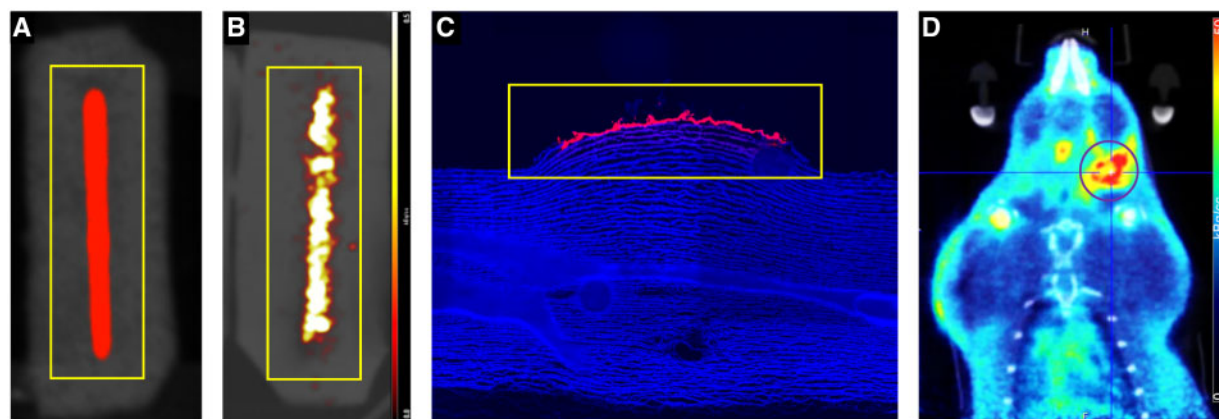


Figure 2 Demonstration of tracer uptake quantification in each experiment. (A and B) Regions of interest placed over the thrombus on the porcine strip in both optical and PET studies are shown, respectively. (C) A cross-section Cy5-ENC2015-labelled thrombus with a ROI placed over the media exposed to blood. The blue fluorescent stain is 4', 6-diamidino-2-phenylindole (DAPI), a commonly used nuclear counterstain to improve immunofluorescence contrast. (D) An ^{18}F -ENC2015 ROI placed over area of uptake within the rat left common carotid artery. ROI, region of interest

three rats with 4 h of whole-body dynamic PET imaging after tail vein injection of ^{18}F -ENC2015 (17.6 ± 1.8 MBq, mean \pm SD). Analysis of radiometabolites generated *in vivo* using HPLC was performed in a further two rats after tail vein injection of ^{18}F -ENC2015 (63.1 ± 19.2 MBq, mean \pm SD) with arterial blood sampled at 2, 30, and 60 min post-radiotracer injection. About 1 mL of rat blood was manually collected at each time-point to generate a population curve. Following blood collection, all samples were kept on ice until analysed. Radioactivity in whole blood and plasma was assessed using a well-type γ -counter using a 400–1400 keV window (Perkin Elmer Wizzard 2, USA). Plasma samples (400 μL) were processed by acetonitrile denaturation and analysed by HPLC (Ultimate 2000, Thermo Fisher, UK) on a Luna C18(2) column (Luna C18(2), 10×250 mm, $10 \mu\text{m}$, Phenomenex, UK) with a mobile phase of acetonitrile and water at a flow rate of 4 mL/min to estimate the parent fraction. A gradient elution from 95% water/5% acetonitrile to 5% water/95% acetonitrile over 12 min was used. Mobile phases were prepared with 0.1% trifluoroacetic acid.

Thrombosis was induced in three rats following application of 10% ferric chloride to the left common carotid artery.¹⁶ After a period of 10 min, ^{18}F -ENC2015 (32.7 ± 2.7 MBq, mean \pm SD, $n = 3$) was injected as a bolus intravenous tail vein injection and animals underwent dynamic PET imaging up to 3 h post-injection. Animals were killed with overdose of anaesthesia. From one animal, the thrombosed carotid was harvested after sacrifice for autoradiographic analysis as for the human thrombus.

Whole-body PET images were re-binned as follows: 7×1 , 2×5 , and 4×10 min per bed position. Dynamic PET images were re-binned as follows: 18×10 s, 2×30 s, 1×60 s, 2×2 min, 10×5 min, and 9×10 min. A CT scan (semi-circular full trajectory, maximum field of view, 480 projections, 50 kVp, 300 ms, and 1:4 binning) was acquired at the end of each emission scan to correct for attenuation and allow PET and CT image co-registration. All PET images were reconstructed using Mediso's iterative Tera-Tomo 3D reconstruction algorithm and the following settings: four iterations, six subsets, full detector model, low regularization, spike filter on, voxel size 0.4 mm and 400–600 keV energy window. PET data were corrected for random coincidences, scatter, and attenuation.

Image processing and analysis

After 24 h of fixation, macroscopic porcine strip fluorescence (Biospace lab photon IMAGER) was determined by placing equal-sized regions of interest over the thrombus in each experimental group and allowing 5 s exposure in the Cy5 channel (Figure 2A). Following this, the proximal and distal 1 mm of the exposed strip were discarded, and the remainder cut into 8 segments. Each segment was subsequently snap-frozen with $5 \mu\text{m}$ sections prepared. Between 4 and 8 microscopic cross-sections were then examined for thrombus fluorescence (Axioscan, Z1) in the Cy5 channel using equally sized regions of interest placed over the thrombus (Figure 2C).

After micro-PET/CT imaging, PET and CT images of the aortic strips were reconstructed, and radiotracer uptake was quantified on PMOD 3.405 software (PMOD Technologies, Switzerland). Equally sized volumes of interest (VOIs) were drawn over the thrombus and uptake quantified as kBq/mL (Figure 2B). To account for variation in infused radioactivity between experiments tracer uptake was normalized by dividing the total uptake within the VOI by the total infused activity in MBq to give kBq/mL/MBq. Autoradiographic images of human and rodent thrombus sections were exported into Fiji software¹⁷ where equally sized region of interest's were drawn on serial sections across each treatment group and greyscale pixel intensity was calculated and compared between groups. Percentage specific binding (%SB) was calculated by subtracting measured activity in tissue sections incubated with different inhibitors (non-labelled ENC2015, scrambled peptide and iodoacetamide) from sections exposed to ^{18}F -ENC2015 only.

Animal PET images were fused with CT images to enable accurate co-registration. In the animals undergoing biodistribution analysis, VOIs were manually drawn around organs of interest and in the thrombus model group, VOIs were drawn around the thrombosed carotid artery, contralateral patent vessel and skin incision site (Figure 2D). Time-activity curves were generated and standardized uptake values (SUVs) calculated as concentration in the VOI divided by injected dose divided by the animal weight. Additionally, SUVs in each volume of interest were divided by the corresponding left ventricular blood pool activity to give SUV ratios (SUVr) and allow quantification of target:non-target ratios.

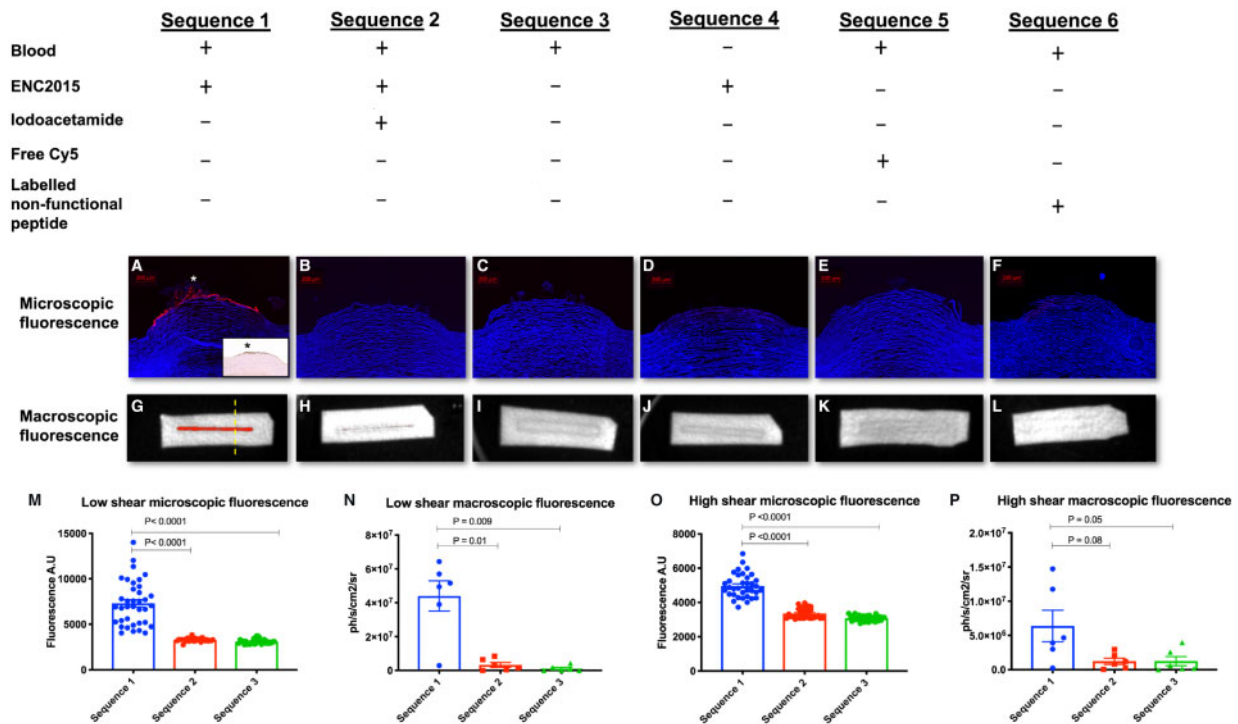


Figure 3 Binding of Cy5-ENC2015 to acutely formed human thrombus. (A–F) Histological cross-sections of the porcine aortic strips at $\times 20$ magnification (sectioned at yellow dotted line in panel G). (G–L) Macroscopic fluorescence of the corresponding sections above is demonstrated. Note clear thrombus fluorescence in A and G with corresponding brightfield direct antibody stain to factor XIIIa (A inset). (M–P) Sequence 1 in bar charts demonstrates the tracer binding to both low and high shear thrombi and how this is specifically blocked by the administration of a factor XIII inhibitor (Sequence 2) and how it can clearly be distinguished from the autofluorescence of blood (Sequence 3). Values expressed as mean \pm SEM, $n = 6$ (paired two-way ANOVA). Asterisk shows thrombus enhancement on histological cross-sections.

For all studies, continuous variables are reported as mean \pm standard error of the mean, unless otherwise indicated in the text. Statistical analysis was performed by two-way analysis of variance with repeated measures and *post hoc* Dunnett's or two-tailed Student's paired *t*-test (GraphPad Prism, version 7.0, Graph Pad Software, USA).

Results

ENC2015 binds to acute human thrombus

Optical fluorescence

In both high and low shear thrombi, Cy5 labelled ENC2015 rapidly bound to acutely formed thrombus (Figure 3A and G) with co-infusion of iodoacetamide strongly inhibiting thrombus fluorescence (Figure 3B and H). Control experiments of blood only (Figure 3C and I) and ENC2015 without blood (Figure 3D and J) showed low levels of fluorescence in comparison to Cy5-ENC2015 (Table 1). Reagent controls (Figure 3E, F, K, and L) also showed low levels of fluorescence in comparison with Cy5-ENC2015.

Positron emission tomography

Similar to the optical study, ^{18}F -ENC2015 demonstrated avid uptake to acutely formed human thrombus (Figure 4A and B) that was specific

for Factor XIIIa with uptake in both high and low shear thrombi strongly inhibited by iodoacetamide (Table 2, Figure 4E and F). Uptake of ^{18}F -ENC2015 was greater in low shear than high shear thrombi (0.96 vs. 0.5 kBq/mL/MBq, $P = 0.02$). After co-infusion of iodoacetamide, ^{18}F -ENC2015 thrombus binding was markedly reduced by 88% and 87% for low and high shear thrombi, respectively. Autoradiographic sections of human thrombus ($n = 3$) showed marked uptake of ^{18}F -ENC2015 (Figure 4C) specifically blocked with unlabelled ENC2015 standard (Figure 4D and Supplementary data online, Figure S4Bii). Thrombus binding was reduced by 67% in low and 64% in high shear thrombi (Figure 4G) and 52% for rodent carotid thrombus harvested from the *in vivo* model. Heterologous blocking with a scrambled peptide showed a mean thrombus binding reduction of 20% in human thrombus and 18% in rodent carotid thrombus (Supplementary data online, Figure 4Biii and S5Aiii). The alkylating agent iodoacetamide had no effect on uptake in both human and rodent explanted thrombus (Supplementary data online, Figure 4iv).

^{18}F -ENC2015 is rapidly cleared from non-target tissues and has slow metabolism *in vivo*

Using HPLC, *in vivo* detection of radiometabolites in rat blood found 100% of the parent compound present at 2 min after intravenous bolus administration, $69.7 \pm 9.8\%$ after 30 min and $42.0 \pm 0.5\%$ after 60 min, with only one other peak indicating a single major polar

Table 1 Optical tracer uptake in *ex vivo* translational model of human thrombus formation

Sequence	ENC2015 + blood (Sequence 1)	ENC2015 + blood + inhibitor (Sequence 2)	Blood only (Sequence 3)	P value (1 vs. 2)	P value (1 vs. 3)
fluorescence					
Low shear macroscopic (ph/s/cm ² /sr)	$4.4 \times 10^7 \pm 0.89 \times 10^7$	$0.33 \times 10^7 \pm 0.13 \times 10^7$	$1.16 \times 10^7 \pm 0.67 \times 10^7$	0.01	0.01
Low shear microscopic (AU)	7307 ± 403	3297 ± 30	3103 ± 48	<0.0001	<0.0001
High shear macroscopic (ph/s/cm ² /sr)	$6.38 \times 10^6 \pm 2.3 \times 10^6$	$1.22 \times 10^6 \pm 0.45 \times 10^6$	$1.24 \times 10^6 \pm 0.67 \times 10^6$	0.09	0.05
High shear microscopic (AU)	4966 ± 118	3356 ± 53	3078 ± 29	<0.0001	<0.0001

Each row represents thrombus type and quantification method used to analyses tracer uptake with each column representing the constituents of each experimental run. Tracer uptake in Sequence 1 (blood + tracer) was significantly greater than 2 (blood + tracer + inhibitor) and 3 (blood only) in all thrombi bar the macroscopically analysed high shear thrombi. Data are shown as mean ± SEM ($n = 6$; paired two-way ANOVA).

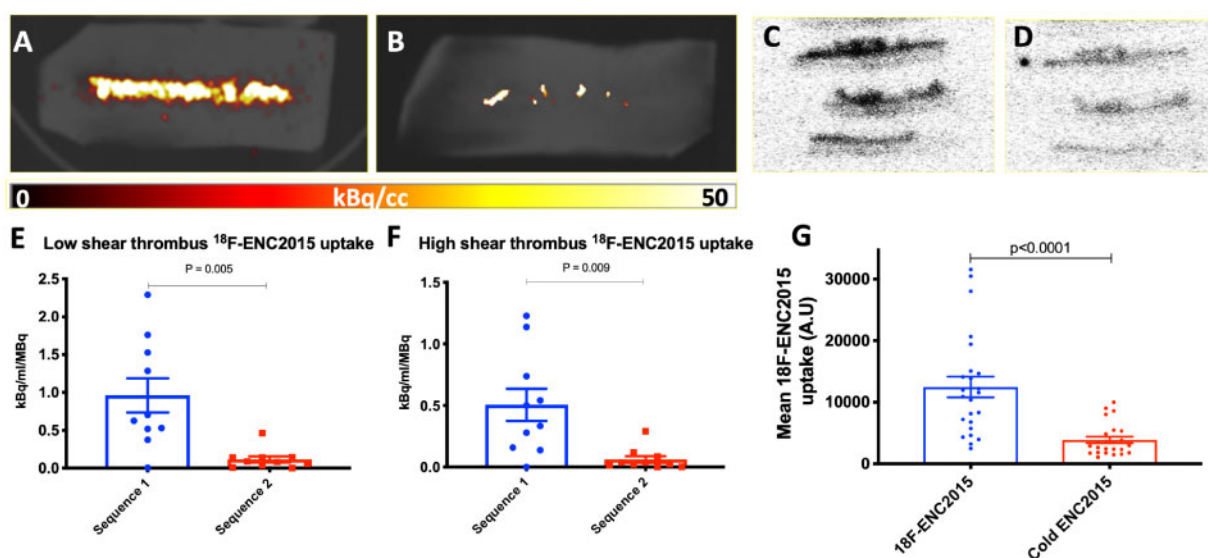


Figure 4 Binding of ¹⁸F-ENC2015 to acutely formed human thrombus. (A) Avid thrombus binding of ¹⁸F-ENC2015 on Micro-PET CT similar to optical version of ENC2015. (B) Diminished thrombus uptake of the radiotracer in the presence of factor XIIIa inhibitor. (C) An autoradiographic plate showing uptake of ¹⁸F-ENC2015 on sections (5 μm thickness) of freshly formed human thrombus. (D) Corresponding serial sections pre-treated with cold tracer demonstrating specific inhibition of binding sites. Bar charts (E + F) demonstrate ¹⁸F-ENC2015 tracer uptake in both low and high shear thrombi (Sequence 1) and how this is specifically blocked by a factor XIII inhibitor (Sequence 2) ($n = 10$). (G) Bar chart shows a marked and significant reduction in ¹⁸F-ENC2015 uptake in human thrombus co-incubated to unlabelled tracer ($n = 3$). Values expressed as mean ± SEM, (paired *t*-test).

radiometabolite (Figure 5A–D). In all animals, ¹⁸F-ENC2015 was rapidly cleared from the vascular bed, heart, and lungs and was predominantly excreted via the kidneys (Supplementary data online, Figure S5). The mean percentage of total injected ¹⁸F-ENC2015 in each major organ over time can be seen in Table 2. Radiometabolite analysis of *ex vivo* human blood using HPLC found the parent ¹⁸F-ENC2015 compound to remain unmetabolized after 8 h post-incubation (Supplementary data online, Figure S3).

¹⁸F-ENC2015 binds to thrombus *in vivo*

Rapid and high uptake of ¹⁸F-ENC2015 was observed in the carotid thrombus and skin incision site in all animals (Figure 6B and C). Mean thrombus SUV_r began to surpass contralateral vessel SUV_r 10 min

after injection. Thrombus SUV_r peaked at 130 min with separation of the activity curves maintained after 180 min post-radiotracer administration (Figure 6C). Mean activity in the thrombosed vessel was higher than in contralateral vessel from 35 to 180 min ($P < 0.0001$, paired *t*-test).

Discussion

Here, we presented the synthesis and pre-clinical evaluation of ENC2015, a dual-purpose optical and PET Factor XIIIa targeted probe for detecting thrombi. In a translational model of deep vascular injury, we successfully demonstrated rapid and SB of ENC2015 to

human thrombus. Fluorescence and ^{18}F -ENC2015 uptake in low shear thrombi were markedly greater than in high shear thrombi which reflect greater fibrin deposition and factor XIIIa activity in acutely formed thrombi formed in a slow flowing venous system.^{18,19}

Table 2 Organ biodistribution of ^{18}F -ENC2015 over time

% ID	1 h	4 h
Heart	0.071 ± 0.016%	0.009 ± 0.001%
Lungs	0.061 ± 0.006%	0.014 ± 0.003%
Kidneys	16.542 ± 1.113%	14.938 ± 0.645%
Bladder	33.498 ± 4.769%	17.14 ± 3.564%
Liver	0.107 ± 0.025%	0.031 ± 0.015%
Brain	0.011 ± 0.001%	0.001 ± 0.0002%

Note the rapid reduction in decay corrected percentage of injected radioactivity from 1 h to 4 h in all analysed organs. Tracer accumulation was greatest in the kidneys owing to a renal site of metabolism and excretion. Data are shown as mean ± SEM ($n = 3$).

However, uptake of both probes was easily appreciable in the high shear, classically platelet-rich 'white thrombus'²⁰ illustrating the versatility of ENC2015 to identify both venous and arterial thrombi. To further enhance understanding of the relationship between fibrin deposition and platelet binding in both high and low shear thrombi, a comparison of ENC2015 with a platelet binding probe such as that reported by Kim *et al.*⁷ would be insightful.

Previous work on NC100668 deduced the major site of metabolism to be the renal cortex with a small fraction metabolized by proteases in the blood.^{8,11,21} Given the chemical similarity between the two peptides, it is likely that ENC2015 would undergo similar metabolic pathways as NC100668. Our analysis found the production of one major *in vivo* metabolite (Metabolite A, Figure 5, Graph C + D). This compound was only identified from *in vivo* rat blood sampling and was not found after 8 h of ^{18}F -ENC2015 incubation in *ex vivo* human blood. This demonstrates that uptake within human thrombus formed in the Badimon chamber studies must therefore be due to the activity of the parent compound and not a human blood-formed metabolite. Furthermore, it highlights the stability of

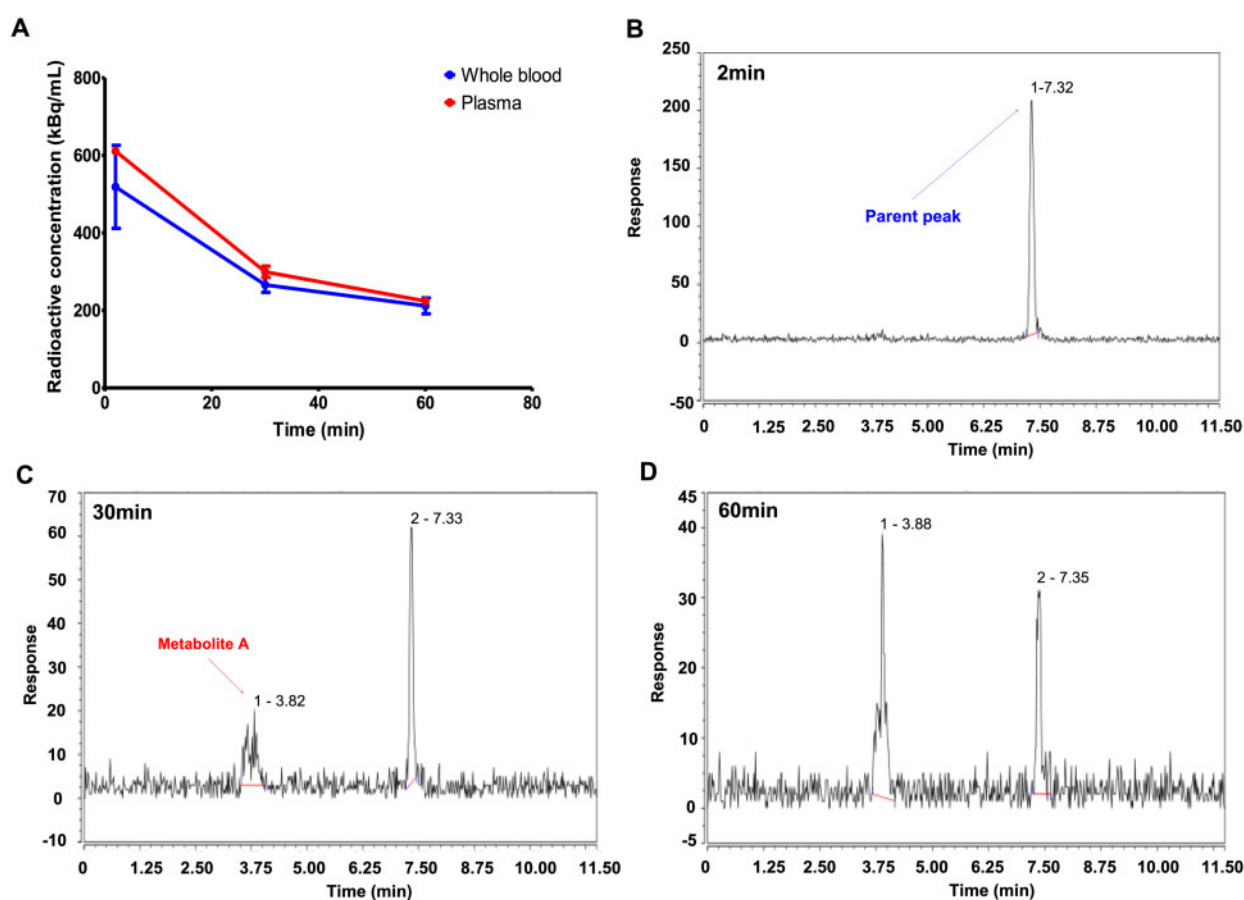
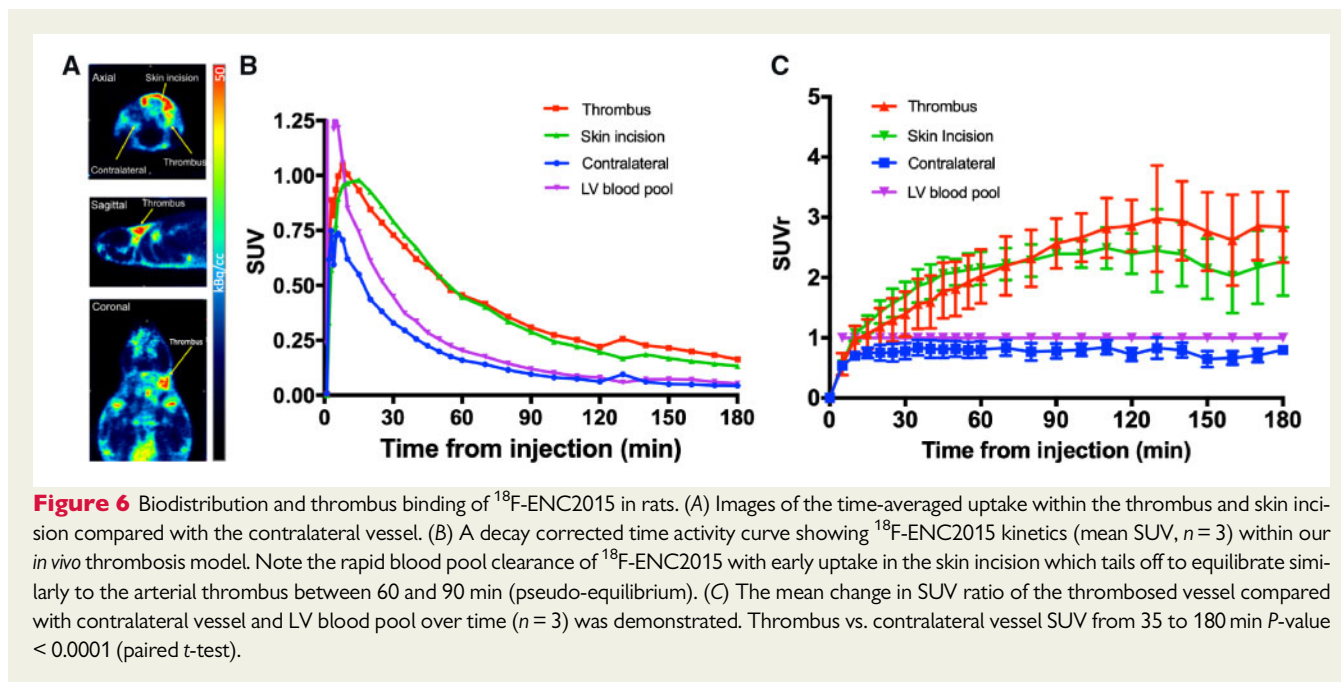


Figure 5 *In vivo* metabolism of ^{18}F -ENC2015 in rat blood. (A) Graph shows the radioactive concentration of ^{18}F -ENC2015 over time in rat whole blood and plasma ($n = 2$). (B) HPLC analysis in chromatogram shows a single peak of parent compound after 2 min of *in vivo* ^{18}F -ENC2015 circulation. (C) After 30 min, a second smaller peak 'metabolite A' can be appreciated on chromatogram. (D) At 60 min, chromatogram shows the radioactivity of metabolite A surpassing that of the parent compound.



^{18}F -ENC2015 in human blood and (in conjunction with *in vivo* biodistribution data showing renal cortex concentration) is consistent with a renal site of metabolism previously reported in both rats and humans.¹¹ Importantly, (and consistent with our *in vivo* findings), plasma clot uptake assays from Edwards et al.¹⁰ using $^{99\text{m}}\text{Tc}$ -NC100668 reported this single major metabolite to have little impact on clot imaging ability.

Forty percent of total injected ^{18}F -ENC2015 remained stable *in vivo* after 1 h incubation which compares with 60% of another promising potentially translatable fibrin probe studied in rats, ^{111}In -FBP15, but is lower than ^{64}Cu -FBP8 (>95%).²² Unlike these probes, ENC2015 is labelled with fluorine-18, which has a half-life of 110 min (compared with 12.7 h for copper-64 and 2.8 days for Indium-111) thereby reducing effective residency times in organs for equal dose regimens and enhancing image quality owing to the more favourable physical decay characteristics of fluoride-18 vs. copper-64 or indium-111. When compared with SPECT, fluoride-18 PET imaging also provides better sensitivity through improved image resolution, shorter scan time and more straightforward quantification.^{23,24} Furthermore, when compared with conventional ^{18}F -labelling, the aluminium fluoride method provides greater yields more rapidly and is flexible for virtually any peptide NOTA structure.²⁵

In the well-validated ferric chloride model of rodent arterial thrombosis,^{16,26} *in vivo* efficacy of ^{18}F -ENC2015 thrombus binding was demonstrated with favourable thrombus to blood pool ratios. Tracer uptake within the thrombosed vessel was greater than the contralateral vessel from 10 min to 2 h after injection, confirming ^{18}F -ENC2015 as a highly sensitive early marker of fibrin crosslinking.^{6,27} Importantly thrombus to blood pool SUVr were maintained between 2:1 and 3:1 after 3 h of dynamic imaging, indicating ongoing FXIIIa dependent fibrin crosslinking and easily appreciable discrimination of thrombus from healthy tissue at 3 h. Finally, autoradiographic studies of human and rodent thrombus showed clear selectivity of ^{18}F -

ENC2015 to target both human and rodent thrombus albeit with some degree of non-SB (which is not uncommon for small peptides exposed to fixed tissue).²⁸ Factor XIIIa is responsible for formation of covalent crosslinks between residues of target proteins, stabilizing the fibrin clot structures through crosslinking of fibrin polymers to increase stiffness, reduce stretch, and limit plasmin-mediated proteolysis. Previous studies have shown factor XIIIa is expressed in joints and the levels of this coagulation transglutaminase changes during osteo-articular diseases. In agreement with those previous observations, the PET signal measured in the joints with ^{18}F -ENC2015 (Figure 2D) is consequent of target expression at those sites.²⁹

^{18}F -ENC2015 thrombus to background SUVr were similar to rat intra cardiac thrombus binding of fibrin probe ^{64}Cu -FBP8 (reported by Blasi et al.^{22,30}) but less than ^{111}In -FBP15 as assessed by SPECT (which reached thrombus to contralateral SUVr of greater than 4:1). Whilst, we explored the role of ^{18}F -ENC2015 in occlusive carotid arterial thrombi, tracer localization to the surgical skin incision demonstrated similar (but not identical) binding profile. This is important for two reasons; more rapid uptake within the skin incision and an earlier plateau than the arterial thrombosis (Figure 6B and C) supports our Badimon chamber findings of greater uptake within acutely formed low shear, fibrin rich thrombi. However, uptake within the arterial thrombus surpasses the skin incision with time illustrating the dichotomous process of fibrin cross-linking in the two vascular spaces. Conversely, the similarity of the binding profiles between skin incision and arterial thrombus renders non-specific tracer pooling from a reservoir or 'leaky vessel' effect unlikely. This unique binding pattern reinforces the versatility of our chosen peptide. This is clinically relevant as constituent differences form the rationale behind differing drug targets for arterial and venous thromboses. Thrombi rich in actively cross-linking fibrin are more prone to therapeutic lysis with tissue plasminogen activators than those that have completed crosslinking.³¹ Correspondingly, thrombi propagated by rapid

platelet activation are more likely to respond to anti-platelet therapy, therefore, identification of both processes may be useful to inform decision making to determine optimal time points for drug therapy.

Whilst single modality PET imaging appears to hold promise in the field of cardiovascular thrombus imaging, the combination of dual labelled probes incorporating advantages of both optical and PET tracers is also now possible.^{32–34} Once bound to their target the decay of a fluorophore depends on exposure time to a specific wavelength of light. Typically, this is very slow meaning tissue can be histologically characterized sometime afterwards if required. Ultimately dual-labelled agents could be used for diagnosis, treatment and procedural planning, therapeutic monitoring, and validation of histological findings; an exciting prospect for the future.

Conclusion

Overall our pre-clinical evaluation has shown that ¹⁸F-ENC2015 is a selective fibrin directed radiotracer which is rapidly cleared from background tissues, excreted predominantly via the urinary system with potential for highly sensitive and specific imaging of both venous and arterial thrombi. Investigation of radiolabelled FXIIIa probes like ¹⁸F-ENC2015 has the potential to improve our understanding of real-time thrombus formation in both arterial and venous systems. Furthermore, the use of thrombus radiotracers may increase diagnostic accuracy and allow optimization of anti-thrombotic and anti-coagulant therapies across a broad spectrum of thrombotic disorders.

Supplementary data

Supplementary data are available at *European Heart Journal - Cardiovascular Imaging* online.

Acknowledgements

The authors would like to thank Adrian Thomson and the Histology department in The Queens Medical Research Institute for their help with histological and fluorescence analysis.

Funding

This work was supported by the British Heart Foundation (RG/16/10/32375), J.P.M.A. (FS/17/51/33096), A.A.S.T. (RG/16/10/32375 and IRF reference 34354, CRM 0024777), and D.E.N. (CH/09/002, RE/18/5/34216, and RG/16/10/32375) are supported by the British Heart Foundation. D.E.N. is the recipient of a Wellcome Trust Senior Investigator Award (WT103782AIA). M.R.D. is supported by the Sir Jules Thorn Biomedical Research Award 2015 (15/JTA) and by the British Heart Foundation (FS/14/78/31020). The study was conducted in Edinburgh Clinical Research Facility and Edinburgh Imaging which are supported by the National Health Service Research Scotland (NRS) through National Health Service Lothian Health Board.

Conflict of interest: Edinburgh Molecular Imaging holds the intellectual property of the ¹⁸F and optical agents. Other authors have no conflict of interest to declare. C.P. is an employee of EMI Ltd.

References

- Wendelboe AM, Raskob GE. Global burden of thrombosis: epidemiologic aspects. *Circ Res* 2016;**118**:1340–7.
- Litmanovich D, Bankier AA, Cantin L, Raptopoulos V, Boisselle PM. CT and MRI in diseases of the aorta. *AJR Am J Roentgenol* 2009;**193**:928–40.
- Kronzon I, Tunick PA. Aortic atherosclerotic disease and stroke. *Circulation* 2006;**114**:63–75.
- Markel A, Weich Y, Gaitini D. Doppler ultrasound in the diagnosis of venous thrombosis. *Angiology* 1995;**46**:65–73.
- Dobrucki LW, Sinusas AJ. PET and SPECT in cardiovascular molecular imaging. *Nat Rev Cardiol* 2010;**7**:38–47.
- Ay I, Blasi F, Rietz TA, Rotile NJ, Kura S, Brownell AL *et al.* *In vivo* molecular imaging of thrombosis and thrombolysis using a fibrin-binding positron emission tomographic probe. *Circ Cardiovasc Imaging* 2014;**7**:697–705.
- Kim C, Lee JS, Han Y, Chae SY, Jin S, Sung C *et al.* Glycoprotein IIb/IIIa receptor imaging with ¹⁸F-GP1 PET for acute venous thromboembolism: an open-label, nonrandomized, phase 1 study. *J Nucl Med* 2019;**60**: 244–9.
- Skotland T, Hustvedt SO, Oulie I, Jacobsen PB, Friisk GA, Langøy AS *et al.* Nc100668, a new tracer for imaging of venous thromboembolism: disposition and metabolism in rats. *Drug Metab Dispos* 2005;**34**:111–20.
- Toft KG, Oulie I, Skotland T. Quantification of NC100668, a new tracer for imaging of venous thromboembolism, in human plasma using reversed-phase liquid chromatography coupled with electrospray ionization ion-trap mass spectrometry. *J Chromatogr B Analyt Technol Biomed Life Sci* 2005;**829**:91–6.
- Edwards D, Lewis J, Battle M, Lear R, Farrar G, Barnett DJ *et al.* (99m)Tc-NC100668, a new tracer for imaging venous thromboemboli: pre-clinical biodistribution and incorporation into plasma clots *in vivo* and *in vitro*. *Eur J Nucl Med Mol Imaging* 2006;**33**:1258–65.
- Edwards D, Battle M, Lear R, Farrar G, Barnett DJ, Godden V *et al.* The *in vivo* and *in vitro* metabolic profile of 99mTc-NC100668, a new tracer for imaging venous thromboembolism: identification and biodistribution of the principal radiolabeled metabolite. *Drug Metab Dispos* 2006;**34**:1128–35.
- Wilson S, Ismat F, Narayan H, Raftis J, Gray T, Cerra M *et al.* Protease-activated receptor type 4 (PAR-4) antagonism with BMS-986120 selectively inhibits human thrombus formation under conditions of high shear stress. *Circulation* 2016;**134**: 18771.
- Lucking AJ, Chelliah R, Trotman AD, Connolly TM, Feuerstein GZ, Fox KA *et al.* Characterisation and reproducibility of a human *ex vivo* model of thrombosis. *Thromb Res* 2010;**126**:431–5.
- Lucking AJ, Gibson KR, Paterson EE, Faratian D, Ludlam CA, Boon NA *et al.* Endogenous tissue plasminogen activator enhances fibrinolysis and limits thrombus formation in a clinical model of thrombosis. *Arterioscler Thromb Vasc Biol* 2013;**33**:1105–11.
- Lucking AJ, Lundbäck M, Barath SL, Mills NL, Sidhu MK, Langrish JP *et al.* Particle traps prevent adverse vascular and prothrombotic effects of diesel engine exhaust inhalation in men. *Circulation* 2011;**123**:1721–8.
- Kurz KD, Main BV, Sandusky GE. Rat model of arterial thrombosis induced by ferric chloride. *Thromb Res* 1990;**60**:269–80.
- Schindelin J, Arganda-Carreras I, Frise E, Kaynig V, Longair M, Pietzsch T *et al.* Fiji: an open-source platform for biological-image analysis. *Nat Methods* 2012;**9**: 676–82.
- Aleman MM, Walton BL, Byrnes JR, Wolberg AS. Fibrinogen and red blood cells in venous thrombosis. *Thromb Res* 2014;**133** Suppl 1:S38–40.
- Houshmand S, Salavati A, Hess S, Ravina M, Alavi A. The role of molecular imaging in diagnosis of deep vein thrombosis. *Am J Nucl Med Mol Imaging* 2014;**4**: 406–25.
- Welsh JD, Muthard RW, Stalker TJ, Taliaferro JP, Diamond SL, Brass LF. A systems approach to hemostasis: 4. How hemostatic thrombi limit the loss of plasma-borne molecules from the microvasculature. *Blood* 2016;**127**:1598–605.
- Toft KG, Johnson JA, Oulie I, Skotland T. NC100668, a new tracer tested for imaging of venous thromboembolism: pharmacokinetics and metabolism in humans. *Drug Metab Dispos* 2007;**35**:1979–84.
- Oliveira BL, Blasi F, Rietz TA, Rotile NJ, Day H, Caravan P. Multimodal molecular imaging reveals high target uptake and specificity of ¹¹¹In- and ⁶⁸Ga-labeled fibrin-binding probes for thrombus detection in rats. *J Nucl Med* 2015;**56**: 1587–92.
- Reader AJ, Zaidi H. Advances in PET image reconstruction. *PET Clin* 2007;**2**: 173–90.
- Rahmim A, Zaidi H. PET versus SPECT: strengths, limitations and challenges. *Nucl Med Commun* 2008;**29**:193–207.
- Laverman P, McBride WJ, Sharkey RM, Goldenberg DM, Boerman OC. Al(18) F labeling of peptides and proteins. *J Labelled Comp Radiopharm* 2014;**57**:219–23.

26. Li W, Nieman M, Sen Gupta A. Ferric chloride-induced murine thrombosis models. *J Vis Exp* 2016;**115**. doi:10.3791/54479.
27. Uppal R, Catana C, Ay I, Benner T, Sorensen AG, Caravan P. Bimodal thrombus imaging: simultaneous PET/MR imaging with a fibrin-targeted dual PET/MR probe—feasibility study in rat model. *Radiology* 2011;**258**:812–20.
28. Dapson RW. Macromolecular changes caused by formalin fixation and antigen retrieval. *Biotech Histochem* 2007;**82**:133–40.
29. Raghu H, Cruz C, Rewerts CL, Frederick MD, Thornton S, Mullins ES et al. Transglutaminase factor XIII promotes arthritis through mechanisms linked to inflammation and bone erosion. *Blood* 2015;**125**:427–37.
30. Blasi F, Oliveira BL, Rietz TA, Rotile NJ, Naha PC, Cormode DP et al. Multisite thrombus imaging and fibrin content estimation with a single whole-body PET scan in rats. *Arterioscler Thromb Vasc Biol* 2015;**35**:2114–21.
31. Brommer EJ, Potter van Loon BJ, Rijken DC, van Bockel JH. Composition and susceptibility to thrombolysis of pathological human arterial thrombi. *Ann N Y Acad Sci* 1992;**667**:283–5.
32. Lütje S, Rijpkema M, Goldenberg DM, van Rij CM, Sharkey RM, McBride WJ et al. Pretargeted dual-modality immuno-SPECT and near-infrared fluorescence imaging for image-guided surgery of prostate cancer. *Cancer Res* 2014;**74**:6216–23.
33. Lütje S, Rijpkema M, Helfrich W, Oyen WJ, Boerman OC. Targeted radionuclide and fluorescence dual-modality imaging of cancer: preclinical advances and clinical translation. *Mol Imaging Biol* 2014;**16**:747–55.
34. Zhang H, Desai P, Koike Y, Houghton J, Carlin S, Tandon N et al. Dual-modality imaging of prostate cancer with a fluorescent and radiogallium-labeled gastrin-releasing peptide receptor antagonist. *J Nucl Med* 2017;**58**:29–35.